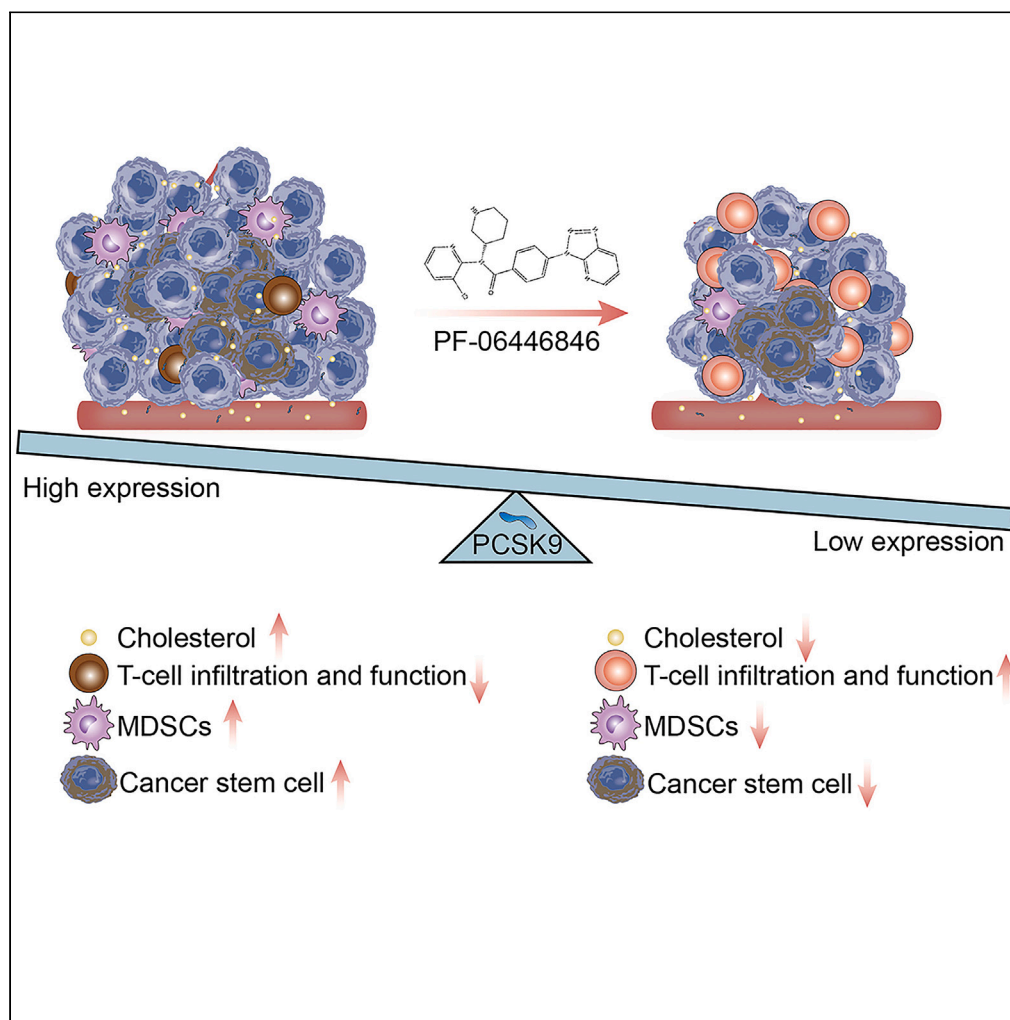


Article

Targeting PCSK9 reduces cancer cell stemness and enhances antitumor immunity in head and neck cancer



Qi-Chao Yang,
Shuo Wang, Yuan-
Tong Liu, ..., Shu-
Cheng Wan, Hui-
Min Li, Zhi-Jun Sun

lhmy@whu.edu.cn (H.-M.L.)
sunzj@whu.edu.cn (Z.-J.S.)

Highlights

Expression of PCSK9 is associated with decreasing survival in human HNSCC

PCSK9 inhibition reduce the stemness of HNSCC in a LDLR-dependent manner

PCSK9 expression increase MDSC and reduce CD8⁺ T cell infiltration and function in tumor

Article

Targeting PCSK9 reduces cancer cell stemness and enhances antitumor immunity in head and neck cancer

Qi-Chao Yang,¹ Shuo Wang,¹ Yuan-Tong Liu,¹ An Song,¹ Zhi-Zhong Wu,¹ Shu-Cheng Wan,¹ Hui-Min Li,^{1,*} and Zhi-Jun Sun^{1,2,3,*}

SUMMARY

Proprotein convertase subtilisin/kexin type 9 (PCSK9) has been demonstrated to play a critical role in regulating cholesterol homeostasis and T cell antitumor immunity. However, the expression, function, and therapeutic value of PCSK9 in head and neck squamous cell carcinoma (HNSCC) remain largely unexplored. Here, we found that the expression of PCSK9 was upregulated in HNSCC tissues, and higher PCSK9 expression indicated poorer prognosis in HNSCC patients. We further found that pharmacological inhibition or siRNA downregulating PCSK9 expression suppressed the stemness-like phenotype of cancer cells in an LDLR-dependent manner. Moreover, PCSK9 inhibition enhanced the infiltration of CD8⁺ T cells and reduced the myeloid-derived suppressor cells (MDSCs) in a 4MOSC1 syngeneic tumor-bearing mouse model, and it also enhanced the anti-tumor effect of anti-PD-1 immune checkpoint blockade (ICB) therapy. Together, these results indicated that PCSK9, a traditional hypercholesterolemia target, may be a novel biomarker and therapeutic target to enhance ICB therapy in HNSCC.

INTRODUCTION

Head and neck squamous cell carcinoma (HNSCC) is the most common malignancy originating from mucosa epithelia in the oral cavity, pharynx, and larynx, with risk factors including smoking, drinking, and human papillomavirus (HPV) infection.^{1,2} Surgery, radiotherapy, and chemotherapy are the principal and traditional therapeutic modalities of HNSCC.¹ In recent years, although new promising therapeutic modalities, including oncolytic therapy and immunotherapy, have been approved for HNSCC,³ the five-year survival rate of patients has improved modestly due to recurrence or metastasis.^{4,5} Therefore, exploring new potential therapeutic targets and better understanding their function in tumorigenesis would be helpful to improve HNSCC patient survival.

Studies have shown that alterations in cholesterol metabolism homeostasis occur frequently in tumorigenesis and development.^{6–9} Furthermore, preclinical studies have indicated that targeting cholesterol metabolism-associated molecules effectively inhibits tumor growth, reprograms the tumor immune microenvironment, and reinvigorates antitumor immunity.^{8,10,11} Proprotein convertase subtilisin/kexin type 9 (PCSK9), as a pivotal molecule in regulating cholesterol metabolism homeostasis, promotes the lysosomal degradation of low-density lipoprotein receptor (LDLR), which contributes to the elevation of plasma lipid profiles.¹² PCSK9 antibodies (evolocumab and alirocumab) have been approved for patients with hypercholesterolemia by the Food and Drug Administration.^{13–16} In the past several years, PCSK9 has also been reported to be overexpressed in many cancer types and to play an important role in tumorigenesis and development, which could promote cancer cell proliferation, inhibit apoptosis, and contribute to tumor recurrence or therapeutic resistance.^{17–19} Furthermore, studies have also found that PCSK9 expression in tumors reduces the major histocompatibility protein class I (MHC-I) expression in tumor cells or mediates T cell receptor degradation.^{20,21} PCSK9 inhibition promotes the intratumoral infiltration of cytotoxic T cells and enhances the antitumor effect of immunotherapy.^{20,22} However, the expression, function and potential therapeutic value of PCSK9 in HNSCC remain largely unexplored. More importantly, studies have shown that obesity and associated genes are associated with unfavorable prognosis in early stage HNSCC patients and that a high-fat diet promotes tumorigenesis by recruiting myeloid-derived suppressor cells

¹The State Key Laboratory Breeding Base of Basic Science of Stomatology (Hubei-MOST) & Key Laboratory of Oral Biomedicine Ministry of Education, School & Hospital of Stomatology, Wuhan University, Wuhan, China

²Department of Oral and Maxillofacial Head Neck Oncology, School & Hospital of Stomatology, Wuhan University, Wuhan, China

³Lead contact

*Correspondence: lhmbj@whu.edu.cn (H.-M.L.), sunjz@whu.edu.cn (Z.-J.S.)
<https://doi.org/10.1016/j.isci.2023.106916>



(MDSCs) in an HNSCC mouse model.²³ Therefore, it is important to explore the potential therapeutic value of this approved lipid-lowering target in HNSCC.

In this study, we found that PCSK9 was upregulated in HNSCC compared to dysplasia or normal mucosa, and that higher expression level of PCSK9 is associated with poorer prognosis or patients with chemotherapy or recurrence. Functionally, the reduction in PCSK9 expression levels dampened the stemness-like phenotype of cancer cells and rescued the impairment of CD8⁺ T cell function. Furthermore, we found that inhibition of PCSK9 significantly delayed tumor growth and enhanced CD8⁺ T cell infiltration and function, and it also potentiated the antitumor effect of anti-PD-1 immune checkpoint blockade (ICB) therapy in an HNSCC 4MOSC1 tumor-bearing mouse model. These findings demonstrated that PCSK9 is a key regulator in cancer cell stemness and highlighted the potential therapeutic value of PCSK9 inhibitors in HNSCC.

RESULTS

Higher expression of PCSK9 is correlated with poorer prognosis of HNSCC patients

To investigate the expression, clinicopathological and prognostic significance of PCSK9 in HNSCC, we utilized the HNSCC tissue microarray for immunohistochemistry and analysis. As shown in [Figures 1A and 1B](#), PCSK9 expression was significantly upregulated in HNSCC tissues compared to dysplasia and normal mucosa, which was consistent with PCSK9 RNA expression results in the HNSCC cohort in The Cancer Genome Atlas (TCGA) database ([Figure S1A](#)). Furthermore, we also detected the expression of PCSK9 in human HNSCC tumor tissues and cell lines (SCC9, SCC4, SCC25, and CAL27) by Western blot analysis, and the results also showed that PCSK9 expression was upregulated in HNSCC tumor tissues or cell lines compared to normal oral mucosa tissues or cell lines ([Figures 1C and 1D](#)). We further analyzed the relationship between PCSK9 expression and clinicopathological parameters. As shown in [Figures 1A and 1E](#), the expression of PCSK9 was positively correlated with the pathological grade, while patients with higher pathological grades tended to have higher PCSK9 expression. Moreover, patients with recurrence or patients treated with TPF chemotherapy (Taxol, platinum and 5-fluorouracil) tended to have higher PCSK9 expression than primary HNSCC patients ([Figures 1F and 1G](#)). However, lymph node metastasis, tumor stage, HPV infection, smoking and drinking status did not influence PCSK9 expression in HNSCC ([Figures S1B–S1F](#)). Finally, we evaluated the prognostic value of PCSK9 expression in HNSCC, and Kaplan-Meier survival analysis indicated that patients with higher PCSK9 expression tended to have a poorer prognosis ([Figure 1H](#)). Furthermore, multivariate survival analysis, which included parameters, such as PCSK9 expression, tumor stage, pathological grade, lymph node metastasis, smoking, drinking, and HPV infection status, also identified that PCSK9 expression function as an independent prognostic indicator in HNSCC patients ([Table 1](#)). Given the important role in regulating cholesterol metabolism homeostasis of PCSK9,¹² we also explored the relationship between clinicopathological parameters and lipid profiles. As shown in [Figures S2A–S2C](#), the results indicated that the levels of lipid profiles have no correlation with pathological grade, lymph node metastasis, and tumor stages in HNSCC patients. Interestingly, we found patients with a higher level of total cholesterol (TC) or LDL-C tend to have a higher expression of PCSK9 in tumors than patients with a normal level of TC or LDL-C ([Figure S2D](#)), indicating that HNSCC patients with hypercholesterolemia may be more sensitive to PCSK9 inhibitor treatment.

PCSK9 inhibition reduce the stemness-like phenotype of HNSCC cell lines in a LDLR-dependent manner

Studies have shown that cancer stem cells are associated with recurrence and chemoresistance in HNSCC.^{24,25} Given that PCSK9 expression was closely related to recurrence and chemotherapy, we further explored whether PCSK9 influences the stem-like phenotype of HNSCC. First, we analyzed the relationship between PCSK9 and proteins associated with the stem-like phenotype by a human HNSCC tissue microarray. The results indicated that PCSK9 expression was closely and positively correlated with cancer stem cell markers, including Bmi1, ALDH1, CD44, CD133, and SOX2 ([Figures 2A, S3A, S3B, and S3C](#)). We then used a highly selective inhibitor of PCSK9 translocation (PF-06446846) to explore the influence of downregulating PCSK9 expression on the stem-like phenotype of cancer cells. As shown in [Figure S3D](#), dual-color immunofluorescence staining of PCSK9 and cancer stem cell marker CD44 in SCC4 cells showed that the PCSK9 inhibitor significantly downregulated the expression of PCSK9 and CD44. Furthermore, Western blot analysis also demonstrated that PCSK9 inhibition in SCC4 cells significantly reduced the expression of CD44 and Bmi1 ([Figure 2B](#)). We also found that PCSK9 expression was elevated in spheroids ([Figure 2C](#)). The sphere formation ability of SCC7 cells was significantly reduced after treatment with the PCSK9 inhibitor ([Figure 2D](#)), indicating the important role of PCSK9 in maintaining the stemness phenotype

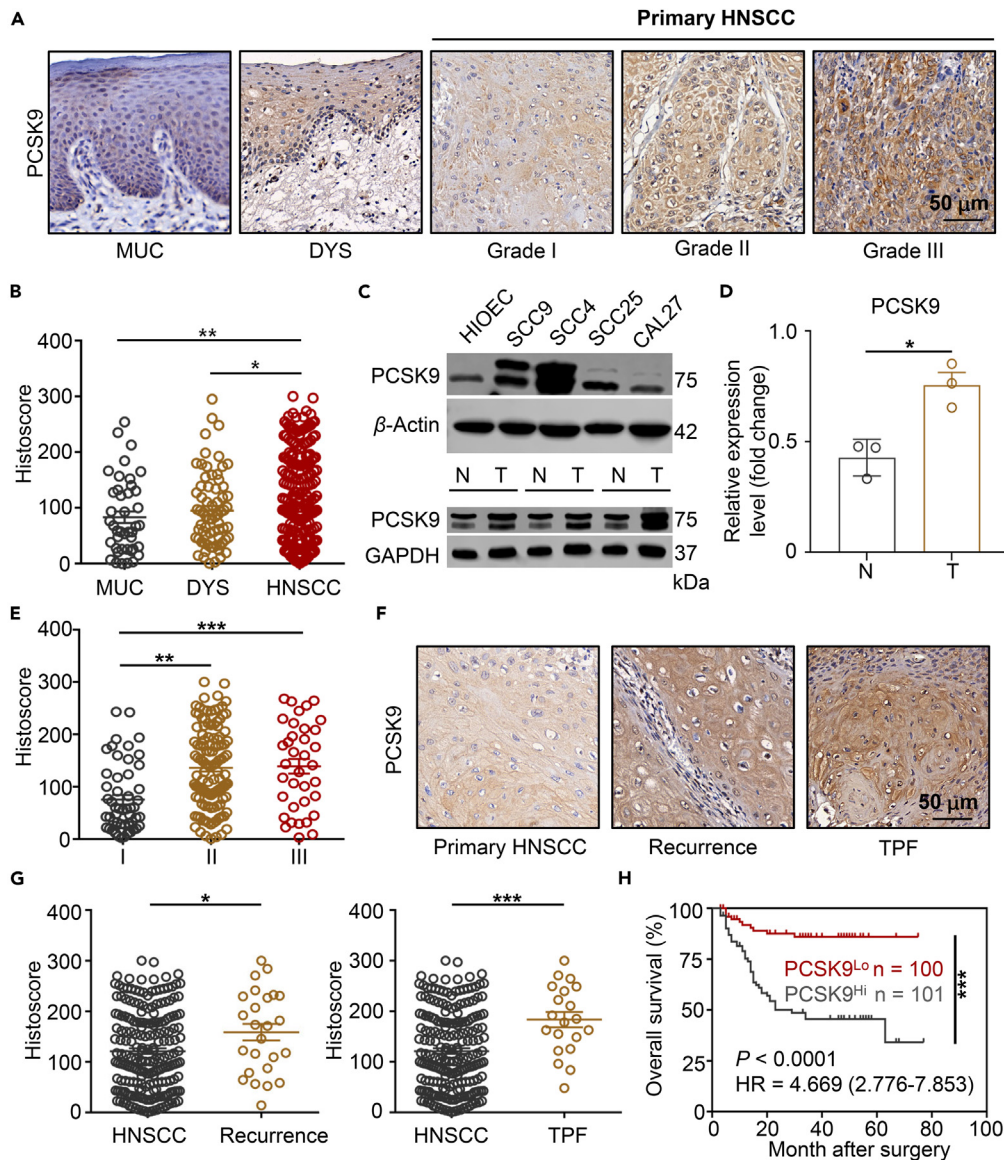


Figure 1. Higher expression of PCSK9 is correlated with poorer prognosis of HNSCC patients

(A) Representative images of PCSK9 immunostaining in HNSCC (grades I, II, and III), dysplasia (DYS), and normal mucosa (MUC).

(B) Quantification of PCSK9 staining in HNSCC (n = 210), DYS (n = 69), and MUC (n = 42).

(C) Protein expression levels of PCSK9 in HNSCC cell lines (SCC9, SCC4, SCC25, and CAL27) and human immortalized oral epithelial cell (HIOEC) or HNSCC tumor tissues (T) and normal oral mucosa (N).

(D) Semiquantitative analysis of PCSK9 expression levels in HNSCC tumor tissues (T) and normal oral mucosa (N) (n = 3).

(E) Quantification of PCSK9 staining quantification in HNSCC (grades I, II, and III) (I, n = 53; II, n = 121; III, n = 36).

(F) Representative images of PCSK9 immunostaining in primary HNSCC, recurrence and TPF chemotherapy.

(G) Quantification of PCSK9 staining in primary HNSCC (n = 210), recurrence (n = 25) and TPF chemotherapy (n = 20).

(H) Kaplan-Meier survival curve of patients with higher PCSK9 expression or lower PCSK9 expression (cutoff = median histoscore of PCSK9). *, p < 0.05; **, p < 0.01; ***, p < 0.001. All error bars represent the SEM. Unpaired t test was used for statistical significance analysis in Figures 1D and 1G. One-way ANOVA followed by Tukey's multiple comparisons was used for statistical significance analysis in Figures 1B and 1E. Log rank test was used for statistical significance analysis in Figure 1H.

of cancer cells. We further utilized a specific siRNA targeting PCSK9 to identify the influence of PCSK9 on the stemness-like phenotype of cancer cells (Figure 2E). Consistently, the results indicated that PCSK9 downregulation significantly reduced the stemness properties of cancer cells (Figure 2F). To further

Table 1. Multivariate analysis for overall survival in primary HNSCC patients

Parameters	HR	95%CI	p value
Smoking	0.792	0.410–1.530	0.488
HPV	1.548	0.499–4.803	0.449
Drinking	0.913	0.462–1.804	0.793
Grade			
II vs. I	2.968	1.001–8.801	0.050
III vs. I	2.035	0.620–6.680	0.242
Tumor size			
T2 vs. T1	1.079	0.460–2.533	0.861
T3 vs. T1	1.706	0.664–4.379	0.267
T4 vs. T1	2.037	0.693–5.984	0.196
Node stage			
N1 vs. N0	0.663	0.310–1.419	0.290
N2 vs. N0	2.220	1.113–4.430	0.024 ^a
PCSK9 expression	4.210	2.087–8.491	0.000 ^a

Cox proportional hazards regression model.

HR, hazard ration, 95% CI, 95% confidence interval.

^a $P < 0.05$.

investigate whether the effect of PCSK9 on cancer cell stemness dependent on LDLR expression, we used a siRNA to reduce the expression of LDLR (Figure 2G). We found that PCSK9 inhibitor could effectively elevate LDLR expression and reduce Bmi1 expression in SCC7 cells, and siRNA downregulating LDLR abolished the effect of PCSK9 inhibitor on Bmi1 and LDLR expression, which indicates that the effect of PCSK9 on cancer cell stemness may dependent on LDLR expression (Figure 2H). Taken together, these results suggested that PCSK9 may play a pivotal role in maintaining the stemness-like phenotype of HNSCC.

PCSK9 is correlated with CD8⁺ T cell exclusion in HNSCC

As a key target in regulating cholesterol homeostasis, PCSK9 has recently been found to play an important role in regulating T cell antitumor immunity in a metabolism-independent manner.^{20,21} Herein, we also explored the role of PCSK9 in T cell antitumor immunity in HNSCC. First, we analyzed the correlations between PCSK9 RNA expression and several T cell infiltration and functional molecules from the HNSCC TCGA database. As shown in Figures 3A–3D and S3E, PCSK9 RNA expression was negatively correlated with RNA expression of T cell markers (CD3E and CD8A) and functional markers (GZMB, PRF1, and IFNG). We further found that patients with higher PCSK9 expression tend to have a lower CD8⁺ T cell infiltration and that the expression of PCSK9 was negatively correlated with CD8 expression in the human HNSCC tissue microarray (Figures 3E and 3F). Consistently, multiplexed immunohistochemistry images also indicated that higher expression of PCSK9 was often accompanied by lower CD8⁺ T cell infiltration (Figure 3G). To further identify the function of PCSK9 in T cell regulation, we created a tumor coculture system with T cells. Interestingly, we found that tumor cells cocultured with CD8⁺ T cells impaired the function of CD8⁺ T cells (GZMB⁺CD8⁺ T and IFN- γ ⁺TNF- α ⁺CD8⁺ T) and that tumor cells pretreated with PCSK9 inhibitor could partly rescue the impairment of CD8⁺ T cell function (Figures 3H and 3I). However, we did not find significant changes in PD-1⁺Tim3⁺ T cells in different groups (Figure S3F). The T cells-mediated tumor killing assay also indicated that CD8⁺ T cells isolated from 4MOSC1-bearing tumor tissues were able to kill more tumor cells (white arrow pointed) pretreated with PCSK9 inhibitor (Figure S3G). Collectively, these results indicated that PCSK9 expression is negatively associated with CD8⁺ T cell infiltration and function in HNSCC.

PCSK9 inhibition delays the tumor growth and enhances the CD8⁺ T cell infiltration and function in 4MOSC1 tumor-bearing mice

To investigate the effect of PCSK9 on HNSCC tumor growth and the immune microenvironment, we utilized the syngeneic HNSCC 4MOSC1 tumor-bearing mouse model for further study.²⁶ The therapeutic strategy is shown in Figure 4A, and the PCSK9 inhibitor was intraperitoneally inoculated every two days

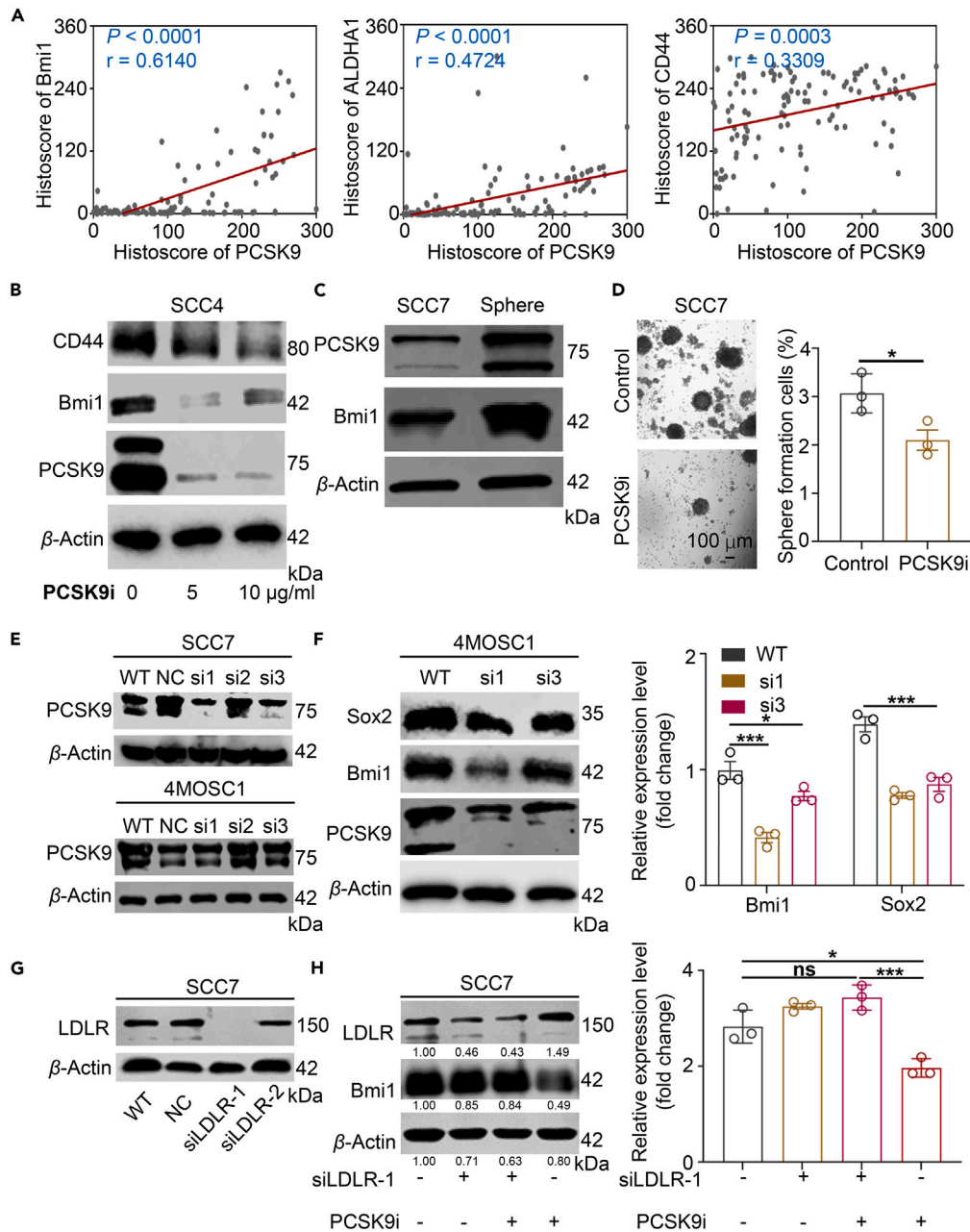


Figure 2. PCSK9 inhibition reduce the stemness-like phenotype of HNSCC cell lines in a LDLR-dependent manner

(A) Correlation between PCSK9 expression and cancer stem cell markers (Bmi1, ALDH1, and CD44) in a human HNSCC tissue microarray by using Spearman's correlation coefficient test ($n = 116$).

(B) Inhibition of PCSK9 with a PCSK9 inhibitor reduced the Bmi1 and CD44 expression.

(C) Expression of PCSK9 and Bmi1 in spheroids and adherent cells.

(D) PCSK9 inhibition reduced the sphere formation ability of SCC7 cells.

(E) siRNA downregulating PCSK9 expression in SCC7 and 4MOSC1 cells as detected by Western blotting.

(F) siRNA downregulating PCSK9 expression reduced cancer stem cell markers (Bmi1 and Sox2).

(G) siRNA downregulating LDLR in SCC7 cell lines.

(H) Inhibition of PCSK9 with a PCSK9 inhibitor in SCC7 cell lines with siLDLR-1 or not. *, $p < 0.05$; ***, $p < 0.001$. All error bar values represent the SEM. Pearson correlation test was used for Figure 2A. Unpaired t test was used for statistical significance analysis in Figure 2D. One-way ANOVA followed by Tukey's multiple comparisons was used for statistical significance analysis in Figures 2F and 2H.

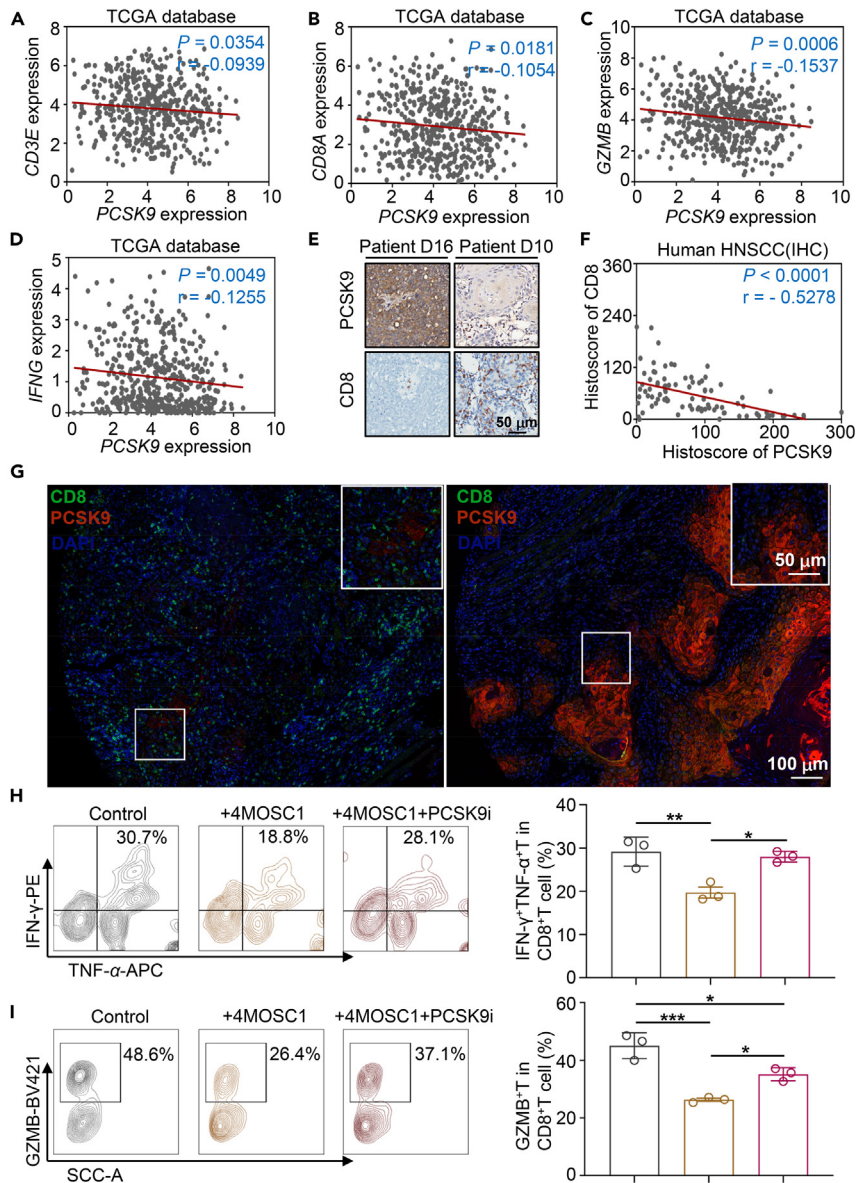


Figure 3. PCSK9 is correlated with CD8⁺ T cell exclusion in HNSCC

(A–D) Correlation between PCSK9 and T cell associated gene (CD3E, CD8A, granzyme B (GZMB), and IFNG) mRNA expression in the HNSCC TCGA database (n = 502).

(E) Representative images indicate that patients with higher PCSK9 expression tended to have lower CD8 T cell infiltration.

(F) Correlation between PCSK9 and CD8 protein expression in a human HNSCC tissue microarray using Spearman's correlation coefficient test (n = 90).

(G) Representative images of multiplexed immunohistochemistry indicated that higher PCSK9 expression was accompanied by lower CD8⁺ T cell infiltration.

(H and I) 4MOSC1 cells pretreated with PCSK9 inhibitor reduced the impairment of CD8⁺ T cells function (GZMB⁺CD8⁺ T and IFN- γ ⁺TNF- α ⁺CD8⁺ T) when cocultured with CD8⁺ T cells. *, p < 0.05; **, p < 0.01; ***, p < 0.001. All error bars represent the SEM. Pearson correlation test was used for Figures 3A–3D and 3F. One-way ANOVA followed by Tukey's multiple comparisons was used for statistical significance analysis in Figures 3H and 3I.

for a total of four times. As shown in Figure 4B, the tumor growth curve indicated that PCSK9 inhibition significantly delayed tumor growth compared to the control group, and the tumor image also identified that PCSK9 inhibition reduced the tumor sizes on mouse tongues (Figures 4B and 4C). Furthermore, as

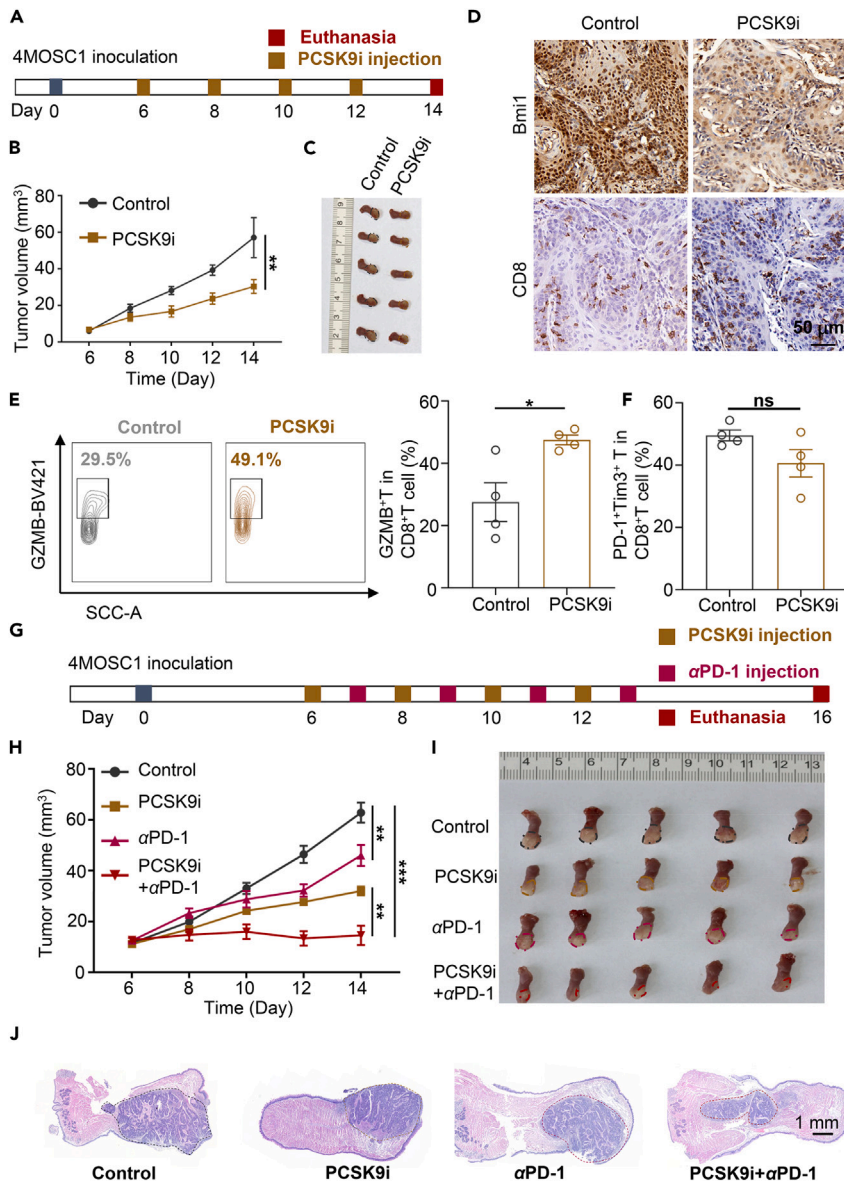


Figure 4. PCSK9 inhibition delays the tumor growth and enhances the CD8⁺ T cell infiltration and function

(A) Scheme illustrating the therapeutic strategy of PCSK9 in 4MOSC1 tumor-bearing mice.
 (B) Tumor volume growth curve of mice treated with PCSK9 inhibitor (5 mg/kg) or PBS.
 (C) Representative tumor images in different groups (n = 5).
 (D) Representative immunohistochemical staining of Bmi1 and CD8 in different groups.
 (E) Representative flow cytometry images and statistical graph of GZMB⁺CD8⁺ T cells in different groups (n = 4).
 (F) Statistical analysis of PD-1⁺CD8⁺ T cells in different groups (n = 4).
 (G) Scheme illustrating the therapeutic strategy of PCSK9 and αPD-1 immunotherapy in 4MOSC1 tumor-bearing mice.
 (H) Tumor volume growth curve of mice treated with PBS, PCSK9 inhibitor (5 mg/kg), αPD-1 immunotherapy, (5 mg/kg) or PCSK9 inhibitor + αPD-1 immunotherapy (n = 5).
 (I) Representative tumor images in different groups (n = 5).
 (J) Representative HE images of tumors in the tongue in different groups. *, p < 0.05; **, p < 0.01; ***, p < 0.001. All error bars represent the SEM. Unpaired t test was used for statistical significance analysis in Figure 4E. Two-way ANOVA was used for statistical significance analysis in Figures 4B and 4H.

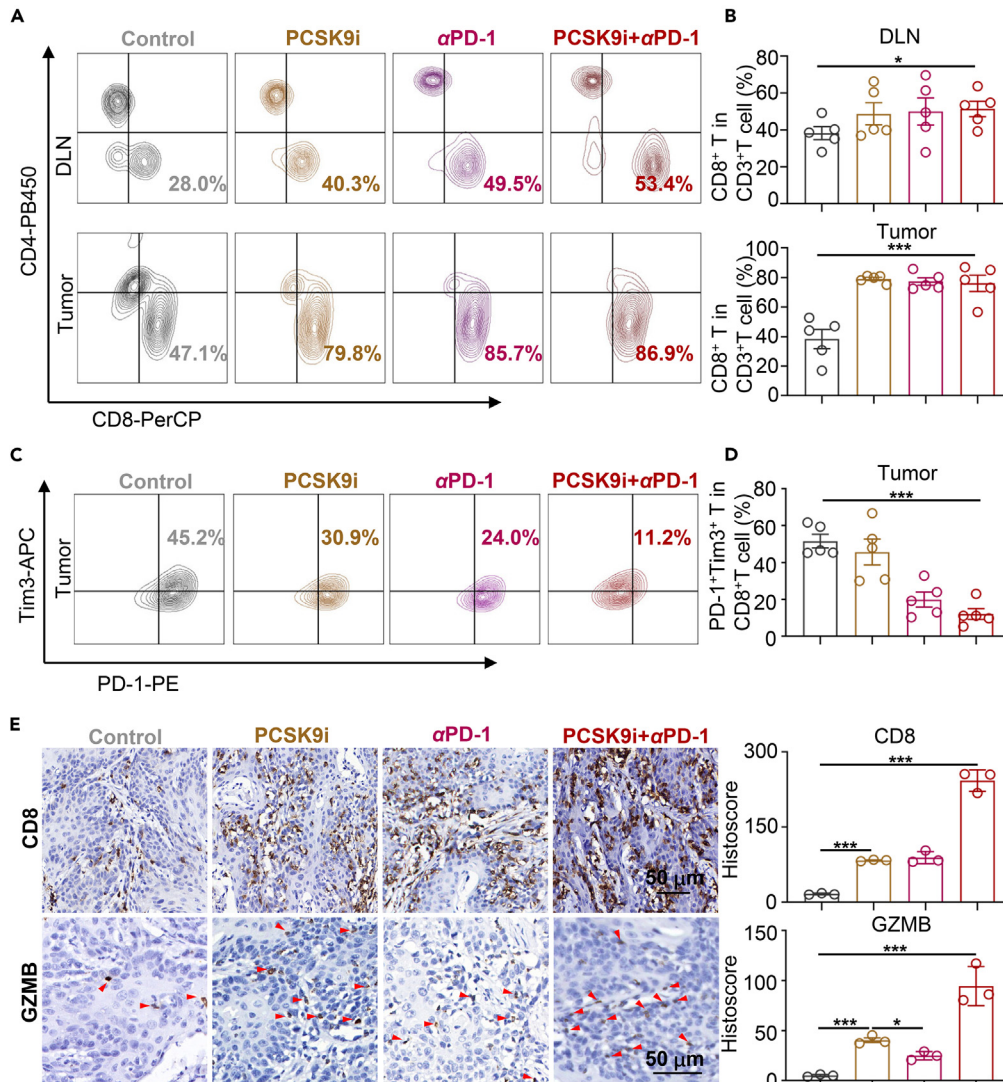


Figure 5. PCSK9 inhibition combined with α PD-1 immunotherapy enhances CD8⁺ T cell infiltration and function

(A) Representative flow cytometry images of CD4⁺ T and CD8⁺ T cells in draining lymph nodes (DLNs) and tumors in different groups.

(B) Statistical analysis of CD4⁺ T and CD8⁺ T cells in different groups (n = 5).

(C) Representative flow cytometry images of Tim3⁺PD-1⁺ T cells in tumors in different groups.

(D) Statistical analysis of Tim3⁺PD-1⁺ T cells in tumors in different groups (n = 5).

(E) Representative immunohistochemical staining and statistical analysis of CD8 and granzyme B (GZMB) in different groups. *, p < 0.05; ***, p < 0.001. All error bars represent the SEM. One-way ANOVA followed by Tukey's multiple comparisons was used for statistical significance analysis in Figures 5B, 5D, and 5E.

PCSK9 plays a pivotal role in regulating cholesterol homeostasis,^{27,28} we also detected the change of total cholesterol and serum circulating PCSK9 levels. Interestingly, we found that PCSK9 inhibition not only effectively reduced the total cholesterol and circulating PCSK9 levels in serum plasma, but also decreased the total cholesterol levels and the expression of Ki-67 in tumor tissues (Figures S3H, S3I, S3J, and S3K). Moreover, consistent with above mentioned results, we found that PCSK9 inhibition remarkably reduced the expression of Bmi1 and enhanced the CD8⁺ T cells infiltration in tumor tissues (Figure 4D). We also found that the proportion of granzyme B⁺CD8⁺ T cells significantly increased in PCSK9 inhibitor treatment group compared to control group, but the proportion of exhausted T (PD-1⁺Tim3⁺ T) cells did not exhibit an obvious decrease (Figures 4E and 4F). Together, these data indicated PCSK9 inhibition effectively delays tumor growth and enhances CD8⁺ T cell infiltration and function in HNSCC.

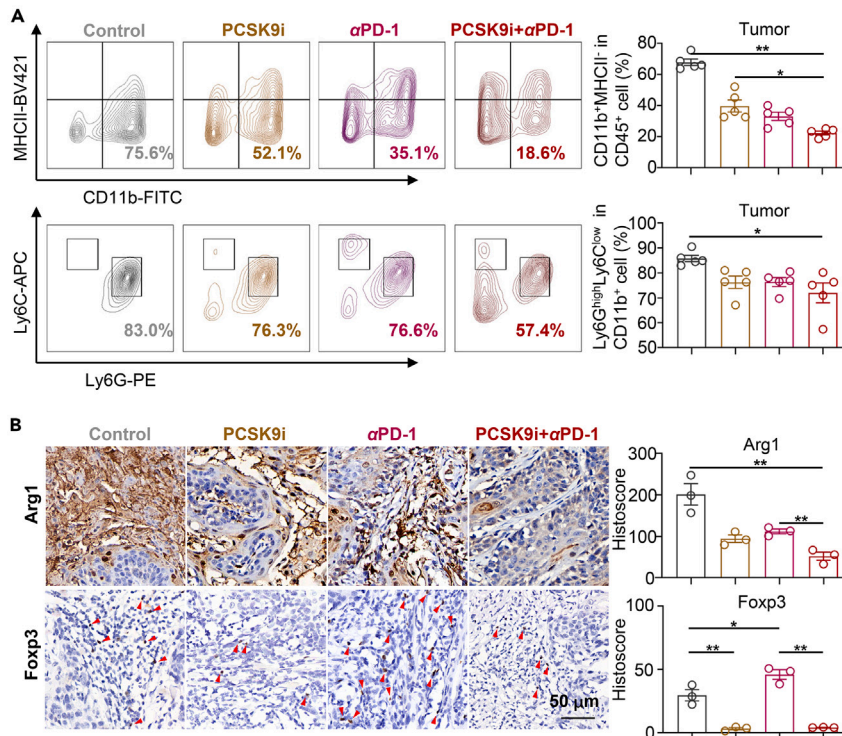


Figure 6. PCSK9 inhibition combined with α PD-1 immunotherapy improves immunosuppressive tumor microenvironment

(A) Representative flow cytometry images and statistical analysis of CD11b⁺MHC-II⁺ and Ly6G^{high}Ly6C^{low} cell populations in different groups (n = 5).

(B) Representative immunohistochemical staining and statistical analysis of Arginase 1 (Arg1) and Foxp3 in different groups (n = 3). *, p < 0.05; **, p < 0.01. All error bars represent the SEM. One-way ANOVA followed by Tukey's multiple comparisons was used for statistical significance analysis in Figures 6A and 6B.

PCSK9 inhibition enhances the antitumor effect of anti-PD-1 (α PD-1) immunotherapy in 4MOSC1 tumor-bearing mice

Encouraged by the enhanced CD8⁺ T cell infiltration, we further explored the potential of combining a PCSK9 inhibitor with T cell-based immunotherapy. The combinational therapeutic strategy of PCSK9 inhibitor and α PD-1 immunotherapy is shown in Figure 4G. Consistent with our expectations, the tumor volume in the PCSK9 inhibitor + α PD-1 group was significantly decreased compared to that in the PCSK9 inhibitor treatment group or α PD-1 immunotherapy group (Figures 4H and S4A). Furthermore, the tumor images and hematoxylin and eosin (HE) sections of the tongue with tumors also demonstrated that the combination group had a smaller tumor size than the monotherapy group (Figures 4I and 4J). To identify the influence of PCSK9 inhibition on tumor, we also took immunochemical staining of LDLR, PCSK9, and rate-limiting enzymes of cholesterol biosynthesis 3-hydroxy-3-methylglutaryl coenzyme A reductase (HMGCR) and sterol regulatory element binding protein-2 (SREBP2) in tumor tissues.^{29,30} As shown in Figure S4B, PCSK9 inhibition significantly reduced expression of PCSK9 and consequently elevated low-density lipoprotein receptor (LDLR) expression in tumors, while α PD-1 immunotherapy has no influence on PCSK9 and LDLR. Consistent with the result from previous report,³¹ the expression of HMGCR and mature SREBP2 (nuclear expression) in tumor tissues also decreased in the PCSK9 inhibition group, which indicated the reduction of cholesterol biosynthesis and maybe associated with the increased expression of LDLR, a receptor for transporting cholesterol to intracellular.^{18,30} We then explored the influence of combination therapy on the immune microenvironment by flow cytometry. As expected, the proportion of CD8⁺ T cells in draining lymph nodes and tumor tissues was significantly increased in the combination group compared to control group (Figures 5A and 5B). Although we did not observe an obvious increase of CD8⁺ T cells in the combination treatment group compared to the monotherapy group, the exhausted T cells (PD-1⁺Tim3⁺ T) in the PCSK9 inhibitor + α PD-1 group were significantly decreased in comparison with the monotherapy group, especially for the PCSK9 inhibitor treatment group (Figures 5C and 5D).

Immunohistochemical staining of CD8 and granzyme B also identified that the combination of PCSK9 inhibitor and α PD-1 immunotherapy effectively promoted the infiltration and enhanced the function of CD8⁺ T cells (Figure 5E). Moreover, we also detected changes in immunosuppressive cell populations in different treatment groups. Surprisingly, we found that both PCSK9 inhibitor and α PD-1 immunotherapy reduced the proportion of CD11b⁺MHC-II⁻ cells and MDSCs (Ly6G^{high}Ly6C^{low}) in tumors, and the combination of PCSK9 inhibitor with α PD-1 immunotherapy exhibited a more marked tendency (Figure 6A). Immunohistochemical staining of arginase 1 (Arg1) also indicated that the PCSK9 inhibitor + α PD-1 group had lighter staining than the monotherapy, which implied a weakened immunosuppressive function of MDSCs (Figure 6B). Furthermore, immunohistochemical staining of Foxp3, a marker of regulatory T (Treg) cells, showed that α PD-1 immunotherapy enhanced the intratumoral infiltration of Tregs and that the PCSK9 inhibitor effectively reduced the Tregs in tumors (Figure 6B). Overall, our results showed that PCSK9 inhibition effectively enhances the antitumor effect and improves antitumor immunity of α PD-1 immunotherapy in 4MOSC1 tumor-bearing mice.

DISCUSSION

PCSK9 is a traditional target in treating hypercholesterolemia due to its function to promote LDLR degradation. In the past several years, studies have shown that PCSK9 also plays an important role in regulating tumor development and antitumor immunity.^{17,20,21,32–35} However, the expression and function of PCSK9 in HNSCC remain largely unexplored. In this study, we found PCSK9 expression was upregulated, and higher expression of PCSK9 indicated a poorer prognosis in HNSCC patients. Furthermore, we found patients with a higher level of TC or LDL-C tend to have a higher expression of PCSK9 in tumor than patients with a normal level of TC or LDL-C. By analyzing PCSK9 expression with clinicopathological information, we also found that PCSK9 expression was positively correlated with pathological grade, while patients with recurrence or patients with chemotherapy tended to have lower PCSK9 expression. PCSK9 was further identified to play a pivotal role in maintaining the stemness-like phenotype of HNSCC. Moreover, we found PCSK9 inhibition reduced total cholesterol level and the proportion of MDSCs and Tregs in tumor tissues as well as enhanced CD8⁺ T cell infiltration and function, and we also demonstrated that PCSK9 inhibition synergistically enhanced the antitumor effect of α PD-1 immunotherapy in a syngeneic HNSCC 4MOSC1 tumor-bearing mice model.

Despite great advances in treatment, HNSCC patients are still confronted with an unsatisfactory five-year survival rate,^{4,36} especially for patients with recurrence or metastasis.³⁶ Therefore, exploring new molecular targets and better understanding their function in tumorigenesis would be helpful for improving HNSCC patient survival. Herein, we found that PCSK9 expression was upregulated in HNSCC compared to normal mucosa or dysplasia, and higher PCSK9 expression indicated a worse pathological grade and a poorer prognosis in HNSCC. As a classical hyperlipidemia-associated molecule, PCSK9 is known for its function in degrading LDLR and elevating cholesterol in serum.^{12,37} However, recent studies have also found that intratumoral PCSK9 is highly expressed in several tumors and associated with patients' poor prognosis.^{17,21,38,39} Additionally, studies have demonstrated that the deregulation of the Janus kinase (JAK)/STAT3 signaling pathway in a chronic inflammatory environment may result in the upregulation of PCSK9.^{40,41} As a result, it is speculated that the chronic inflammatory milieu present in tumors may also be responsible for the elevated expression of PCSK9 in tumors. Furthermore, PCSK9 has also been found to promote cancer cell proliferation, inhibit apoptosis, induce oncogenesis and mediate sorafenib resistance in cancer.^{31,38,42} Together, combining our results, we consider that PCSK9 may be a therapeutic target and prognostic marker in HNSCC.

The stemness phenotype of cancer cells accounts for the recurrence and chemoresistance of HNSCC,^{43–45} and exploring the molecules associated with the stemness phenotype would be helpful for addressing tumor recurrence and chemoresistance.^{46,47} Herein, we found that PCSK9 expression was upregulated in patients with recurrence and TPF chemotherapy. Furthermore, PCSK9 expression was closely and positively correlated with cancer stem cell markers, and PCSK9 inhibition effectively reduced the stemness-like phenotype of HNSCC in an LDLR-dependent manner. Studies have also found that PCSK9 is highly expressed in undifferentiated stem cells⁴⁸ and that it regulates cancer recurrence and metastasis.^{49,50} Moreover, our results also indicated that PCSK9 inhibition could reduce the expression of the rate-limiting enzymes of cholesterol biosynthesis HMGCR and mature SREBP2 by elevating LDLR expression, which are essential for cancer stem cell propagation.^{51,52} Together, we speculate that PCSK9 inhibition could reduce the stemness-like phenotype of HNSCC cell lines by inhibiting cholesterol biosynthesis in an

LDLR-dependent manner and that targeting PCSK9 may efficaciously prevent cancer recurrence or overcome chemoresistance. Although we are the first to report that PCSK9 may function as a therapeutic target to reduce the stemness of cancer cells, the actual mechanisms of PCSK9 regulating the stemness of cancer cells are still unknown, and solid evidence for targeting PCSK9 to regulate cancer recurrence or chemoresistance in HNSCC is still awaiting further study.

Enriched cholesterol in the tumor microenvironment has been reported to induce CD8⁺ T cell exhaustion.^{53,54} Furthermore, a recent study has also reported that a high-fat diet promotes the incidence of HNSCC and confers an immunosuppressive tumor microenvironment.²³ As a key regulator of cholesterol metabolism, PCSK9 has also been reported to play an important role in regulating CD8⁺ T antitumor immunity by reducing MHC-I expression in tumor cells or mediating T cell receptor degradation.^{20,21} Consistently, we found that PCSK9 expression was upregulated and positively associated with CD8⁺ T cell exclusion and dysfunction in HNSCC. Moreover, PCSK9 inhibition also reduced the cholesterol level and enhanced CD8⁺ T cell infiltration and function in 4MOSC1 tumor microenvironment. However, previous studies have shown that CD8⁺ T cell metabolic changes and produces more lactate during activation involving a switch from oxidative phosphorylation to aerobic glycolysis.⁵⁵ And the metabolic changes in CD8⁺ T cells after PCSK9 inhibition in tumor may need further exploration. Interestingly, we also found that inhibition of PCSK9 in 4MOSC1 tumor-bearing mice also reduced the immunosuppressive cell populations of MDSCs and Tregs in the tumor microenvironment, which may be associated with the reduced cholesterol level in tumor microenvironment.^{22,23,56,57} The immunosuppressive tumor microenvironment and insufficient CD8⁺ T cells infiltration are the main reasons for the unexpected therapeutic effect of immunotherapy in cancer.^{58,59} We found that PCSK9 inhibition effectively improved the therapeutic effect of α PD-1 immunotherapy, which may be attributed to the alleviated immunosuppressive cells and elevated CD8⁺ T cells in the tumor microenvironment after PCSK9 inhibition. Furthermore, we found though α PD-1 immunotherapy could reduce MDSCs, another immunosuppressive cell population Tregs was elevated in tumors. This may also provide evidence for combining PCSK9 inhibitor with α PD-1 immunotherapy in HNSCC. However, the detailed mechanism by which PCSK9 inhibition regulates immunosuppressive cell populations MDSCs and Tregs was not investigated in the present study.

In summary, the present results demonstrated that PCSK9 expression functions as an independent prognostic marker and may play a pivotal role in maintaining the stemness-like phenotype of HNSCC. Furthermore, PCSK9 inhibition could effectively enhance CD8⁺ T cell infiltration and reduce the number of immunosuppressive cells MDSCs and Tregs in HNSCC. More importantly, we provided a rationale for combining a new lipid-lowering PCSK9 inhibitor and α PD-1 immunotherapy to enhance antitumor effects in HNSCC. Overall, we found that in addition to lowering blood lipids, PCSK9 inhibitors also reduce the stemness-like phenotype of cancer cells and enhance the therapeutic effect of α PD-1 immunotherapy in HNSCC.

Limitations of the study

In this study, we identified that PCSK9 reduces the stemness-like phenotype of cancer cells and enhances the therapeutic effect of α PD-1 immunotherapy in HNSCC. Although we identified that PCSK9 influences the stemness-like phenotype of HNSCC, the actual mechanism of PCSK9 regulating cancer cell stemness was not investigated. And solid evidence for targeting PCSK9 to regulate cancer recurrence or chemoresistance in HNSCC is still awaiting further study. We also found that PCSK9 inhibition could reduce the MDSCs in tumor microenvironment, but whether it was associated with reduced cholesterol in tumor remains unclear. Furthermore, the concentration of serum PCSK9 and total cholesterol was detected only in three animals for each group, which may contribute to the deviations of results.

STAR★METHODS

Detailed methods are provided in the online version of this paper and include the following:

- KEY RESOURCES TABLE
- RESOURCE AVAILABILITY
 - Lead contact
 - Materials availability
 - Data and code availability
- EXPERIMENTAL MODEL AND SUBJECT DETAILS
 - Animal experiment

- Cell lines
- **METHOD DETAILS**
 - Human samples and tissue microarray construction
 - Immunohistochemistry and quantification
 - Western blot
 - siRNA transfection assay
 - Sphere formation assay
 - Multiplex immunohistochemistry
 - Dual-color immunofluorescence
 - Cell coculture assay
 - T cells-mediated tumor killing assay
 - Antitumor effects of PF-06446846 *in vivo*
 - Flow cytometry
 - Total cholesterol detection assay
- **QUANTIFICATION AND STATISTICAL ANALYSIS**

SUPPLEMENTAL INFORMATION

Supplemental information can be found online at <https://doi.org/10.1016/j.isci.2023.106916>.

ACKNOWLEDGMENTS

This work was supported by National Natural Science Foundation of China 82101042 (H.M.L.), 82273202 (Z.J.S.), 82072996 (Z.J.S.), and 81874131 (Z.J.S.), the Fundamental Research Funds for the Central Universities (2042021kf0176), and Natural Science Foundation of Hubei Province of China (2021CFB107).

AUTHOR CONTRIBUTIONS

Z.J.S. and H.M.L. conceptualized the experiment; Q.C.Y. designed and performed the experiment, analyzed the data, and wrote the manuscript; S.W. and Y.T.L. performed the experiment; A.S. and Z.Z.W. performed the experiment and analyzed the data; S.C.W. supervised the project, provided results interpretation. All the authors read and approved the final manuscript.

DECLARATION OF INTERESTS

The authors declare no competing interests.

Received: December 12, 2022

Revised: March 1, 2023

Accepted: May 14, 2023

Published: May 19, 2023

REFERENCES

1. Johnson, D.E., Burtneš, B., Leemans, C.R., Lui, V.W.Y., Bauman, J.E., and Grandis, J.R. (2020). Head and neck squamous cell carcinoma. *Nat. Rev. Dis. Prim.* 6, 92. <https://doi.org/10.1038/s41572-020-00224-3>.
2. Siegel, R.L., Miller, K.D., Fuchs, H.E., and Jemal, A. (2022). Cancer statistics, 2022. *Ca - Cancer J. Clin.* 72, 7–33. <https://doi.org/10.3322/caac.21708>.
3. Ferris, R.L. (2015). Immunology and immunotherapy of head and neck cancer. *J. Clin. Oncol.* 33, 3293–3304. <https://doi.org/10.1200/JCO.2015.61.1509>.
4. Chi, A.C., Day, T.A., and Neville, B.W. (2015). Oral cavity and oropharyngeal squamous cell carcinoma—an update. *Ca - Cancer J. Clin.* 65, 401–421. <https://doi.org/10.3322/caac.21293>.
5. Cao, B., Patel, K.B., Li, T., Yao, S., Chung, C.H., and Wang, X. (2023). A subnetwork-based framework for prioritizing and evaluating prognostic gene modules from cancer transcriptome data. *iScience* 26, 105915. <https://doi.org/10.1016/j.isci.2022.105915>.
6. Snaebjornsson, M.T., Janaki-Raman, S., and Schulze, A. (2020). Greasing the wheels of the cancer machine: the role of lipid metabolism in cancer. *Cell Metabol.* 31, 62–76. <https://doi.org/10.1016/j.cmet.2019.11.010>.
7. Bovenga, F., Sabbà, C., and Moschetta, A. (2015). Uncoupling nuclear receptor LXR and cholesterol metabolism in cancer. *Cell Metabol.* 21, 517–526. <https://doi.org/10.1016/j.cmet.2015.03.002>.
8. Huang, B., Song, B.L., and Xu, C. (2020). Cholesterol metabolism in cancer: mechanisms and therapeutic opportunities. *Nat. Metab.* 2, 132–141. <https://doi.org/10.1038/s42255-020-0174-0>.
9. Chae, S.Y., Nam, D., Hyeon, D.Y., Hong, A., Lee, T.D., Kim, S., Im, D., Hong, J., Kang, C., Lee, J.W., et al. (2021). DNA repair and cholesterol-mediated drug efflux induce dose-dependent chemoresistance in nutrient-deprived neuroblastoma cells. *iScience* 24, 102325. <https://doi.org/10.1016/j.isci.2021.102325>.
10. Ding, X., Zhang, W., Li, S., and Yang, H. (2019). The role of cholesterol metabolism in cancer. *Am. J. Cancer Res.* 9, 219–227.
11. Gomaschi, M. (2020). Role of lipoproteins in the microenvironment of hormone-dependent cancers. *Trends Endocrinol. Metabol.* 31, 256–268. <https://doi.org/10.1016/j.tem.2019.11.005>.

12. Seidah, N.G., Awan, Z., Chrétien, M., and Mbikay, M. (2014). PCSK9: a key modulator of cardiovascular health. *Circ. Res.* 114, 1022–1036. <https://doi.org/10.1161/CIRCRESAHA.114.301621>.
13. Shapiro, M.D., Tavori, H., and Fazio, S. (2018). PCSK9: from basic science discoveries to clinical trials. *Circ. Res.* 122, 1420–1438. <https://doi.org/10.1161/CIRCRESAHA.118.311227>.
14. Miller, M. (2019). ACC/AHA lipids & ASCVD guidelines: 2018 update. *Metabolism* 99, 116–118. <https://doi.org/10.1016/j.metabol.2019.03.008>.
15. Koskinas, K.C., Gencer, B., Nanchen, D., Branca, M., Carballo, D., Klingenberg, R., Blum, M.R., Carballo, S., Muller, O., Matter, C.M., et al. (2021). Eligibility for PCSK9 inhibitors based on the 2019 ESC/EAS and 2018 ACC/AHA guidelines. *Eur. J. Prev. Cardiol.* 28, 59–65. <https://doi.org/10.1177/2047487320940102>.
16. Carugo, S., Sirtori, C.R., Corsini, A., Tokgozoglul, L., and Ruscica, M. (2022). PCSK9 inhibition and risk of diabetes: should we worry? *Curr. Atherosclerosis Rep.* 24, 995–1004. <https://doi.org/10.1007/s11883-022-01074-y>.
17. Bhattacharya, A., Chowdhury, A., Chaudhury, K., and Shukla, P.C. (2021). Proprotein convertase subtilisin/kexin type 9 (PCSK9): a potential multifaceted player in cancer. *Biochim. Biophys. Acta Rev. Canc* 1876, 188581. <https://doi.org/10.1016/j.bbcan.2021.188581>.
18. Macchi, C., Ferri, N., Sirtori, C.R., Corsini, A., Banach, M., and Ruscica, M. (2021). Proprotein convertase subtilisin/kexin type 9: a view beyond the canonical cholesterol-lowering impact. *Am. J. Pathol.* 191, 1385–1397. <https://doi.org/10.1016/j.ajpath.2021.04.016>.
19. Seidah, N.G., and Prat, A. (2022). The multifaceted biology of PCSK9. *Endocr. Rev.* 43, 558–582. <https://doi.org/10.1210/endo/bnab035>.
20. Liu, X., Bao, X., Hu, M., Chang, H., Jiao, M., Cheng, J., Xie, L., Huang, Q., Li, F., and Li, C.Y. (2020). Inhibition of PCSK9 potentiates immune checkpoint therapy for cancer. *Nature* 588, 693–698. <https://doi.org/10.1038/s41586-020-2911-7>.
21. Yuan, J., Cai, T., Zheng, X., Ren, Y., Qi, J., Lu, X., Chen, H., Lin, H., Chen, Z., Liu, M., et al. (2021). Potentiating CD8(+) T cell antitumor activity by inhibiting PCSK9 to promote LDLR-mediated TCR recycling and signaling. *Protein Cell* 12, 240–260. <https://doi.org/10.1007/s13238-021-00821-2>.
22. Wang, R., Liu, H., He, P., An, D., Guo, X., Zhang, X., and Feng, M. (2022). Inhibition of PCSK9 enhances the antitumor effect of PD-1 inhibitor in colorectal cancer by promoting the infiltration of CD8(+) T cells and the exclusion of Treg cells. *Front. Immunol.* 13, 947756. <https://doi.org/10.3389/fimmu.2022.947756>.
23. Peng, J., Hu, Q., Chen, X., Wang, C., Zhang, J., Ren, X., Wang, Y., Tao, X., Li, H., Song, M., et al. (2021). Diet-induced obesity accelerates oral carcinogenesis by recruitment and functional enhancement of myeloid-derived suppressor cells. *Cell Death Dis.* 12, 946. <https://doi.org/10.1038/s41419-021-04217-2>.
24. Naik, P.P., Das, D.N., Panda, P.K., Mukhopadhyay, S., Sinha, N., Prahara, P.P., Agarwal, R., and Bhutia, S.K. (2016). Implications of cancer stem cells in developing therapeutic resistance in oral cancer. *Oral Oncol.* 62, 122–135. <https://doi.org/10.1016/j.oraloncology.2016.10.008>.
25. Simple, M., Suresh, A., Das, D., and Kuriakose, M.A. (2015). Cancer stem cells and field cancerization of oral squamous cell carcinoma. *Oral Oncol.* 51, 643–651. <https://doi.org/10.1016/j.oraloncology.2015.04.006>.
26. Wang, Z., Wu, V.H., Allevato, M.M., Gilardi, M., He, Y., Luis Callejas-Valera, J., Vitale-Cross, L., Martin, D., Amornphimoltham, P., McDermott, J., et al. (2019). Syngeneic animal models of tobacco-associated oral cancer reveal the activity of in situ anti-CTLA-4. *Nat. Commun.* 10, 5546. <https://doi.org/10.1038/s41467-019-13471-0>.
27. Abifadel, M., Varret, M., Rabès, J.P., Allard, D., Ouguerram, K., Devillers, M., Cruaud, C., Benjannet, S., Wickham, L., Erlich, D., et al. (2003). Mutations in PCSK9 cause autosomal dominant hypercholesterolemia. *Nat. Genet.* 34, 154–156. <https://doi.org/10.1038/ng1161>.
28. Mousavi, S.A., Berge, K.E., and Leren, T.P. (2009). The unique role of proprotein convertase subtilisin/kexin 9 in cholesterol homeostasis. *J. Intern. Med.* 266, 507–519. <https://doi.org/10.1111/j.1365-2796.2009.02167.x>.
29. Waku, T., Hagiwara, T., Tamura, N., Atsumi, Y., Urano, Y., Suzuki, M., Iwami, T., Sato, K., Yamamoto, M., Noguchi, N., and Kobayashi, A. (2021). NRF3 upregulates gene expression in SREBP2-dependent mevalonate pathway with cholesterol uptake and lipogenesis inhibition. *iScience* 24, 103180. <https://doi.org/10.1016/j.isci.2021.103180>.
30. Cao, X., Fang, W., Li, X., Wang, X., Mai, K., and Ai, Q. (2022). Increased LDL receptor by SREBP2 or SREBP2-induced lncRNA LDLR-AS promotes triglyceride accumulation in fish. *iScience* 25, 104670. <https://doi.org/10.1016/j.isci.2022.104670>.
31. Wong, C.C., Wu, J.L., Ji, F., Kang, W., Bian, X., Chen, H., Chan, L.S., Luk, S.T.Y., Tong, S., Xu, J., et al. (2022). The cholesterol uptake regulator PCSK9 promotes and is a therapeutic target in APC/KRAS-mutant colorectal cancer. *Nat. Commun.* 13, 3971. <https://doi.org/10.1038/s41467-022-31663-z>.
32. Almeida, C.R., Ferreira, B.H., and Duarte, I.F. (2021). Targeting PCSK9: a promising adjuvant strategy in cancer immunotherapy. *Signal Transduct. Targeted Ther.* 6, 111. <https://doi.org/10.1038/s41392-021-00530-6>.
33. Lei, L., Li, X., Yuan, Y.J., Chen, Z.L., He, J.H., Wu, J.H., and Cai, X.S. (2020). Inhibition of proprotein convertase subtilisin/kexin type 9 attenuates 2,4,6-trinitrobenzenesulfonic acid-induced colitis via repressing toll-like receptor 4/nuclear factor-kappa B. *Kaohsiung J. Med. Sci.* 36, 705–711. <https://doi.org/10.1002/kjm2.12225>.
34. Liu, X., Suo, R., Chan, C.Z.Y., Liu, T., Tse, G., and Li, G. (2019). The immune functions of PCSK9: local and systemic perspectives. *J. Cell. Physiol.* 234, 19180–19188. <https://doi.org/10.1002/jcp.28612>.
35. He, M., Hu, J., Fang, T., Tang, W., Lv, B., Yang, B., and Xia, J. (2021). Protein convertase subtilisin/kexin type 9 inhibits hepatocellular carcinoma growth by interacting with GSTP1 and suppressing the JNK signaling pathway. *Cancer Biol. Med.* 19, 90–103. <https://doi.org/10.20892/j.issn.2095-3941.2020.0313>.
36. Carlisle, J.W., Steuer, C.E., Owonikoko, T.K., and Saba, N.F. (2020). An update on the immune landscape in lung and head and neck cancers. *Ca - Cancer J. Clin.* 70, 505–517. <https://doi.org/10.3322/caac.21630>.
37. Guedeney, P., Giustino, G., Sorrentino, S., Claessen, B.E., Camaj, A., Kalkman, D.N., Vogel, B., Sartori, S., De Rosa, S., Baber, U., et al. (2019). Efficacy and safety of alirocumab and evolocumab: a systematic review and meta-analysis of randomized controlled trials. *Eur. Heart J.* 43, e17–e25. <https://doi.org/10.1093/eurheartj/ehz430>.
38. Sun, Y., Zhang, H., Meng, J., Guo, F., Ren, D., Wu, H., and Jin, X. (2022). S-palmitoylation of PCSK9 induces sorafenib resistance in liver cancer by activating the PI3K/AKT pathway. *Cell Rep.* 40, 111194. <https://doi.org/10.1016/j.celrep.2022.111194>.
39. Zhang, S.Z., Zhu, X.D., Feng, L.H., Li, X.L., Liu, X.F., Sun, H.C., and Tang, Z.Y. (2021). PCSK9 promotes tumor growth by inhibiting tumor cell apoptosis in hepatocellular carcinoma. *Exp. Hematol. Oncol.* 10, 25. <https://doi.org/10.1186/s40164-021-00218-1>.
40. Ruscica, M., Ricci, C., Macchi, C., Magni, P., Cristofani, R., Liu, J., Corsini, A., and Ferri, N. (2016). Suppressor of cytokine signaling-3 (SOCS-3) induces proprotein convertase subtilisin kexin type 9 (PCSK9) expression in hepatic HepG2 cell line. *J. Biol. Chem.* 291, 3508–3519. <https://doi.org/10.1074/jbc.M115.664706>.
41. Macchi, C., Greco, M.F., Botta, M., Sperandio, P., Dongiovanni, P., Valenti, L., Cicero, A.F.G., Borghi, C., Lupu, M.G., Romeo, S., et al. (2020). Leptin, resistin, and proprotein convertase subtilisin/kexin type 9: the role of STAT3. *Am. J. Pathol.* 190, 2226–2236. <https://doi.org/10.1016/j.ajpath.2020.07.016>.
42. Xu, X., Cui, Y., Cao, L., Zhang, Y., Yin, Y., and Hu, X. (2017). PCSK9 regulates apoptosis in human lung adenocarcinoma A549 cells via endoplasmic reticulum stress and mitochondrial signaling pathways. *Exp. Ther. Med.* 13, 1993–1999. <https://doi.org/10.3892/etm.2017.4218>.
43. Oker, N., Kaufmann, A., and Albers, A. (2012). [Biology and relevance of stem cells in squamous head and neck cancer: latest insights and review of literature].

- Laryngo-Rhino-Otol. 91, 326–335. quiz 333–324. <https://doi.org/10.1055/s-0032-1306364>.
44. Zhang, Z., Filho, M.S., and Nör, J.E. (2012). The biology of head and neck cancer stem cells. *Oral Oncol.* 48, 1–9. <https://doi.org/10.1016/j.oraloncology.2011.10.004>.
45. Das, M., and Law, S. (2018). Role of tumor microenvironment in cancer stem cell chemoresistance and recurrence. *Int. J. Biochem. Cell Biol.* 103, 115–124. <https://doi.org/10.1016/j.biocel.2018.08.011>.
46. Raghav, P.K., and Mann, Z. (2021). Cancer stem cells targets and combined therapies to prevent cancer recurrence. *Life Sci.* 277, 119465. <https://doi.org/10.1016/j.lfs.2021.119465>.
47. Nunes, T., Hamdan, D., Leboeuf, C., El Bouchtaoui, M., Gapihan, G., Nguyen, T.T., Meles, S., Angeli, E., Ratajczak, P., Lu, H., et al. (2018). Targeting cancer stem cells to overcome chemoresistance. *Int. J. Mol. Sci.* 19, 4036. <https://doi.org/10.3390/ijms19124036>.
48. Roudaut, M., Idriss, S., Caillaud, A., Girardeau, A., Rimbert, A., Champon, B., David, A., Lévêque, A., Arnaud, L., Pichelin, M., et al. (2021). PCSK9 regulates the NODAL signaling pathway and cellular proliferation in hiPSCs. *Stem Cell Rep.* 16, 2958–2972. <https://doi.org/10.1016/j.stemcr.2021.10.004>.
49. Abdelwahed, K.S., Siddique, A.B., Qusa, M.H., King, J.A., Souid, S., Abd Elmageed, Z.Y., and El Sayed, K.A. (2021). PCSK9 axis-targeting pseurotin A as a novel prostate cancer recurrence suppressor lead. *ACS Pharmacol. Transl. Sci.* 4, 1771–1781. <https://doi.org/10.1021/acspstsci.1c00145>.
50. Abdelwahed, K.S., Siddique, A.B., Mohyeldin, M.M., Qusa, M.H., Goda, A.A., Singh, S.S., Ayoub, N.M., King, J.A., Jois, S.D., and El Sayed, K.A. (2020). Pseurotin A as a novel suppressor of hormone dependent breast cancer progression and recurrence by inhibiting PCSK9 secretion and interaction with LDL receptor. *Pharmacol. Res.* 158, 104847. <https://doi.org/10.1016/j.phrs.2020.104847>.
51. Ehmsen, S., Pedersen, M.H., Wang, G., Terp, M.G., Arslanagic, A., Hood, B.L., Conrads, T.P., Leth-Larsen, R., and Ditzel, H.J. (2019). Increased cholesterol biosynthesis is a key characteristic of breast cancer stem cells influencing patient outcome. *Cell Rep.* 27, 3927–3938.e6. <https://doi.org/10.1016/j.celrep.2019.05.104>.
52. Gao, S., Soares, F., Wang, S., Wong, C.C., Chen, H., Yang, Z., Liu, W., Go, M.Y.Y., Ahmed, M., Zeng, Y., et al. (2021). CRISPR screens identify cholesterol biosynthesis as a therapeutic target on stemness and drug resistance of colon cancer. *Oncogene* 40, 6601–6613. <https://doi.org/10.1038/s41388-021-01882-7>.
53. Ma, X., Bi, E., Lu, Y., Su, P., Huang, C., Liu, L., Wang, Q., Yang, M., Kalady, M.F., Qian, J., et al. (2019). Cholesterol induces CD8(+) T cell exhaustion in the tumor microenvironment. *Cell Metabol.* 30, 143–156.e5. <https://doi.org/10.1016/j.cmet.2019.04.002>.
54. Picarda, E., Ren, X., and Zang, X. (2019). Tumor cholesterol up, T cells down. *Cell Metabol.* 30, 12–13. <https://doi.org/10.1016/j.cmet.2019.06.007>.
55. Macchi, C., Moregola, A., Greco, M.F., Svecla, M., Bonacina, F., Dhup, S., Dadhich, R.K., Audano, M., Sonveaux, P., Mauro, C., et al. (2022). Monocarboxylate transporter 1 deficiency impacts CD8(+) T lymphocytes proliferation and recruitment to adipose tissue during obesity. *iScience* 25, 104435. <https://doi.org/10.1016/j.isci.2022.104435>.
56. Bleve, A., Durante, B., Sica, A., and Consonni, F.M. (2020). Lipid metabolism and cancer immunotherapy: immunosuppressive myeloid cells at the crossroad. *Int. J. Mol. Sci.* 21, 5845. <https://doi.org/10.3390/ijms21165845>.
57. Yang, Z., Huo, Y., Zhou, S., Guo, J., Ma, X., Li, T., Fan, C., and Wang, L. (2022). Cancer cell-intrinsic XBP1 drives immunosuppressive reprogramming of intratumoral myeloid cells by promoting cholesterol production. *Cell Metabol.* 34, 2018–2035.e8. <https://doi.org/10.1016/j.cmet.2022.10.010>.
58. Sharma, P., Hu-Lieskovan, S., Wargo, J.A., and Ribas, A. (2017). Primary, adaptive, and acquired resistance to cancer immunotherapy. *Cell* 168, 707–723. <https://doi.org/10.1016/j.cell.2017.01.017>.
59. Shelton, S.E., Nguyen, H.T., Barbie, D.A., and Kamm, R.D. (2021). Engineering approaches for studying immune-tumor cell interactions and immunotherapy. *iScience* 24, 101985. <https://doi.org/10.1016/j.isci.2020.101985>.
60. Chen, L., Yang, Q.C., Li, Y.C., Yang, L.L., Liu, J.F., Li, H., Xiao, Y., Bu, L.L., Zhang, W.F., and Sun, Z.J. (2020). Targeting CMTM6 suppresses stem cell-like properties and enhances antitumor immunity in head and neck squamous cell carcinoma. *Cancer Immunol. Res.* 8, 179–191. <https://doi.org/10.1158/2326-6066.CIR-19-0394>.

STAR★METHODS

KEY RESOURCES TABLE

REAGENT or RESOURCE	SOURCE	IDENTIFIER
Antibodies		
anti-PCSK9	abcam	Cat# ab185194
anti-PCSK9	Proteintech	Cat# 27882-1-AP; RRID:AB_2918134
anti-LDLR	Proteintech	Cat# 10785-1-AP; RRID:AB_2281164
Anti-HMGCR	Proteintech	Cat# 13533-1-AP; RRID:AB_2877957
Anti-SRBF2	Proteintech	Cat# 28212-1-AP; RRID:AB_2881091
anti-CD44	CST	Cat# 3570; RRID:AB_2076464
anti-Bmi1	Proteintech	Cat # 10832-1-AP; RRID:AB_2065392
anti-Sox2	CST	Cat# 10652; RRID:AB_2798664
anti-CD133	CST	Cat# 64326; RRID:AB_2721172
anti-ALDHA1	CST	Cat# 54135; RRID:AB_2799452
anti-CD8	CST	Cat# 85336; RRID:AB_2909535
anti-CD8	CST	Cat# 98941; RRID:AB_2756376
anti-Granzyme B	CST	Cat# 46890; RRID:AB_2799313
anti-Arginase 1	CST	Cat# 93668; RRID:AB_2800207
anti-Foxp3	CST	Cat# 12653; RRID:AB_2797979
anti-Ki67	CST	Cat# 12202; RRID:AB_2620142
HRP- conjugated β -actin	Proteintech	Cat# HRP-66009; RRID:AB_2883836
HRP- conjugated GAPDH	Proteintech	Cat# HRP-60004; RRID:AB_2737588
anti-IgG	CST	Cat# 3900; RRID:AB_1550038
eFluor 506 Fixable Viability Dye	eBioscience	Cat# 65-0866-18
APC-Cyanine7 anti-mouse CD45	Biolegend	Cat# 103116; RRID:AB_312981
PE-Cyanine5.5 anti-mouse CD45	eBioscience	Cat# 35-0451-82; RRID:AB_469718
FITC anti-mouse CD3	Biolegend	Cat# 100204; RRID:AB_312661
eFluor™ 450 anti-mouse CD4	eBioscience	Cat# 48-0041-82; RRID:AB_10718983
PerCP anti-mouse CD8a	Biolegend	Cat# 100732; RRID:AB_893423
APC anti-mouse Tim3	Biolegend	Cat# 134008; RRID:AB_2562998
PE anti-mouse PD-1	Biolegend	Cat# 135206; RRID:AB_1877231
FITC anti-mouse CD11b	Biolegend	Cat# 101206; RRID:AB_312789
BV421 anti-mouse MHC-II	eBioscience	Cat# 404-5321-82; RRID:AB_2925530
PE anti-mouse Ly6G	Biolegend	Cat# 127608; RRID:AB_1186099
APC anti-mouse Ly6C	Biolegend	Cat# 128016; RRID:AB_1732076
APC anti-mouse TNF- α	Biolegend	Cat# 506308; RRID:AB_315429
PE anti-mouse IFN- γ	Biolegend	Cat# 505808; RRID:AB_315402
BV421 anti-mouse granzyme b	Biolegend	Cat# 396414; RRID:AB_2810603
Chemicals, peptides, and recombinant proteins		
PF-06446846	MedChemExpress	HY-120088A
RPMI 1640 medium	ThermoFisher	C11875500BT
KSFM serum-free keratinocyte medium	ThermoFisher	10744019
KGM-Gold serum-free keratinocyte medium	LONZA	00192151
hydrocortisone	MedChemExpress	HY-N0583

(Continued on next page)

Continued

REAGENT or RESOURCE	SOURCE	IDENTIFIER
Recombinant mouse IL-2	absin	abs00970
anti-mouse CD3e	BD Bioscience	553238
anti-mouse CD28	BD Bioscience	553294
αPD-1	BioXcell	#BE0146
Lipofectamine 3000	ThermoFisher	L3000008

Critical commercial assays

Multiplex immunohistochemistry	AKOYA Biosciences	NEL811001KT
Total Cholesterol Content Assay kit	Solarbio	BC1985
Cell Stimulation Cocktail	ThermoFisher	00-4975-93
PCSK9 Elisa	Solarbio	SEKM-0243
PCSK9 siRNA	GenePharma	NA
LDLR siRNA	GenePharma	NA
BCA Protein Assay Kit	Beyotime	P0012S
Transcription Factor Buffer Set	BD Biosciences	562574
Flow cytometry sorting	Beckman Coulter	NA

Experimental models: Cell Lines

4MOSC1	J. Silvio Gutkind University of California, San Diego	MTA: sd-2017-202
SCC7	Qian-Ming Chen Sichuan University	NA
SCC4	ATCC	CRL-1624
SCC9	ATCC	CRL-1629
SCC25	ATCC	CRL-1628
CAL27	ATCC	CRL-2095

Experimental models: Organisms/strains

Mouse: C57 BL/6J	Solarbio	N/A
------------------	----------	-----

Oligonucleotides

siRNA PCSK9-1	GenePharma	Pcsk9-mus-964
siRNA PCSK9-2	GenePharma	Pcsk9-mus-1299
siRNA PCSK9-3	GenePharma	Pcsk9-mus-2019
siRNA LDLR-1	GenePharma	LDLR-1
siRNA LDLR-2	GenePharma	LDLR-1

Software and algorithms

GraphPad Prism	GraphPad	Version 9.4.1
Aperio ImageScope	Leica Biosystems	Version 12.3.2
CaseViewer	3DHISTECH	Version 2.4.0
PerkinElmer Vectra	PerkinElmer	Vectra 3.0
flowjo	BD Biosciences	Version 10

Others

Transcriptomic data of HNSCC	TCGA	https://portal.gdc.cancer.gov/
------------------------------	------	---

RESOURCE AVAILABILITY

Lead contact

Further information and requests for resources should be directed to and will be fulfilled by the lead contact, Zhi-Jun Sun (sunj@whu.edu.cn).

Materials availability

This study did not generate new unique reagents.

Data and code availability

- The transcriptomic data for HNSCC samples used for correlation analysis is publicly available from TCGA database (<https://portal.gdc.cancer.gov/>). All data has been included in main figures or supplementary information.
- This paper does not report original code.
- Any additional information required to reanalyze the data reported in this paper is available from the [lead contact](#) upon request.

EXPERIMENTAL MODEL AND SUBJECT DETAILS

Animal experiment

6-8 weeks female C57 BL/6J mice were housed in the Center for Animal Experiment of Wuhan University. And the experiments were approved by the Institutional Animal Care and Use Committee of Wuhan University Center for Animal Experiment (WP20210558).

For the tumor growth studies, 1×10^6 4MOSC1 cells (30 μ l) were inoculated to the tongue of C57 BL/6J mouse to establish the syngeneic HNSCC 4MOSC1 tumor-bearing model. Each group contained five mice. Tumor volume and body weight were calculated every two days. All mice were euthanized on day 16, and tumor and draining lymph node were dissected for further study.

Cell lines

SCC4, SCC9, SCC25 and CAL27 were obtained from ATCC during 2014-2019. And SCC4, SCC9 and SCC25 were cultured in DMEM/F12 medium with 400 ng/ml hydrocortisone and that CAL27 was cultured in DMEM medium. The human immortalized oral epithelial cell (HIOEC) was cultured in KGM-Gold serum-free keratinocyte medium. The mouse HNSCC cell lines SCC7 (gifted by Qian-Ming Chen, Sichuan university) and 4MOSC1 (gifted by J. Silvio Gutkind from University of California, San Diego with materials transfer agreement, MTA: sd-2017-202) were separately cultured in RPMI 1640 medium and KSFM serum-free keratinocyte medium. And all cell lines were tested annually for *mycoplasma* contamination by PCR Detection Kit (C0301S, Beyotime, China).

METHOD DETAILS

Human samples and tissue microarray construction

The collection of human HNSCC tissue samples and construction of tissue microarrays were described as previously reported.⁶⁰ All patients signed the informed consent and that human studies were approved by Medical Ethics Committee of the Hospital of Stomatology, Wuhan University (2016LUNSHENZI62). The human tissue microarrays include 210 primary HNSCC samples, 69 dysplasia and 42 normal mucosae. The tissue microarrays also include 25 recurrent HNSCC samples, 20 HNSCC samples with a history of TPF chemotherapy (Taxol, platinum and 5-fluorouracil) and 15 HNSCC samples with a radiotherapy history. Furthermore, the lipid profiles information of 184 HNSCC patients was acquired from their clinical record. The lipid profiles information included 46 patients with higher concentration of serum triglyceride (TG > 1.71 mmol/L), 36 patients with higher concentration of serum total cholesterol (TC > 5.23 mmol/L), 40 patients with lower concentration of serum high density lipoprotein cholesterol (HDL-C < 0.91 mmol/L), 24 patients with higher concentration of serum low density lipoprotein cholesterol (LDL-C > 3.36 mmol/L) and 91 patients with normal lipid profiles. The clinical follow-up was continuously ongoing until death of the patients or the end of the study and 9 patients were lost during follow-up.

Immunohistochemistry and quantification

The 4- μ m paraffin-embedded tissue sections were baked at 60 °C for 2 h, and then deparaffinized in xylene for 30 min. After rehydrated in an alcohol gradient and subjected to antigen retrieval, the sections were blocked with 3% hydrogen peroxide for 20 min and 10% serum for 30 min. Then, the sections were incubated with indicated antibodies and isotype-matched IgG controls at 4 °C for 12 h and then washed with PBS for 3 times. Thereafter, the sections were successively incubated with a secondary biotinylated

IgG and an avidin–biotin–peroxidase reagent at 37 °C for 20 min, and then, 3,3'-diaminobenzidine tetra-chloride was added to detect the binding of these antibodies with their specific antigens. The sections were scanned with 3D HISTECH Panoramic MIDI and analyzed with CaseViewer software.

Western blot

After incubation with indicated treatment, the cells were collected and lysed with lysis buffer (RIPA, 1mM PMSF) for 20 min, and then centrifuged at 12,000 g for 5 min. The supernatant was collected and the concentration of proteins were measured with BCA Protein Assay Kit (Beyotime Biotechnology, Wuhan, China). After denaturation, equal amounts of proteins were fractionated by 10% SDS-polyacrylamide gel electrophoresis and transferred to polyvinylidene fluoride (PVDF) membranes (Roche Diagnostics GmbH, Mannheim, Germany). The membranes were then blocked with 5% milk for 1 h and incubated with primary antibodies at 4 °C for 12 h. After incubation with the appropriate secondary antibody, the protein blots were treated with chemiluminescent substrates visualized using a chemiluminescent (ECL) detection apparatus to show the expression levels of proteins.

siRNA transfection assay

The PCSK9 siRNA and LDLR siRNA was designed and synthesized by GenePharma (GenePharma, China). SCC7 or 4MOSC1 cells (2×10^5) were seeded in 6-well plates and cultured at 37 °C for 24 h. When cell density reached 50%, the PCSK9 siRNAs or LDLR siRNA (20 nM), Lipofectamine 3000 transfection reagent and Opti-MEM were mixed and incubated for 10 min. After that, the mixture was added to the culture medium and cells were transfected for 6 h. The sequences of PCSK9 siRNA and LDLR siRNA were as follows: siRNA PCSK9-1: 5'-GGAGGUGUAUCUCUAGAUUTT-3', siRNA PCSK9-2: 5'-GGUAUAGCCGCAUCCUCAATT-3', siRNA PCSK9-3: 5'-CCAACUGCAGCAUCCACAATT-3', siLDLR-1: 5'-GAGGUGACCAACAAUAGAATT-3', siLDLR-2: 5'-AACAUACUGGACAGAUUTT-3'.

Sphere formation assay

SCC7 cells (1×10^3) were seeded in 6-well Ultra-Low Attachment Microplates (Costar, Corning, USA) in sphere culture medium (DMEM/F12 + 1% N2 supplement + 1% B27 + 20 ng/ml bFGF + 20 ng/ml EGF) with PCSK9 inhibitor (5 µg/ml) or not. After cultured for 14 days, we used the invert microscope to take pictures and calculate the number of spheroids larger than 100 µm.

Multiplex immunohistochemistry

An Opal Multiplex Immunohistochemical Detection Kit was utilized in this experiment. The 4-µm paraffin-embedded tissue sections were baked at 60 °C for 2 h, and then deparaffinized in xylene for 30 min. After rehydrated in an alcohol gradient and subjected to antigen retrieval, the tissue sections were incubated with blocker to block the non-specific binding. Then primary antibodies, Opal polymer horseradish peroxidase (HRP) and tyramide signal amplification (TSA) were sequentially added to the tissue sections. After antibody stripping with heat microwave, the sections were subjected to the blocker, primary antibodies, Opal polymer HRP and TSA repeatedly until the last antibody incubation. Finally, the sections were stained with DAPI for nuclear counterstaining. The sections were scanned with a PerkinElmer Vectra.

Dual-color immunofluorescence

After treatment with PCSK9 inhibitor (5 µg/ml), the adherent SCC4 cells were washed with cold PBS for 3 times. Then, cells were fixed with 4% paraformaldehyde for 15 min and subsequently washed with PBS for 3 times. After treated with 0.5% Triton-X100 for rupturing membranes, primary antibody and appropriate fluorescent secondary antibody were sequentially incubated with cells. Then the steps above were repeated for another primary antibody from different species. Finally, the cells were stained with DAPI for nuclear counterstaining. Inverted fluorescence microscope was used to observe the cells and capture images.

Cell coculture assay

We first acquired lymphocytes from mouse lymph nodes by grinding and filtering under asepsis condition and then obtained CD8⁺ T cells by flow cytometry (Moflo XDP, Beckman Coulter, USA). 96-well U-bottom plate was coated with an anti-mouse CD3e (10 µg/ml) (BD Bioscience, 553238) at 4 °C for 12 h and washed 3 times with PBS to remove the non-bound soluble antibody. Subsequently, 1×10^5 Lymphocytes mixed with 2×10^4 4MOSC1 cells pretreated with PCSK9 inhibitor (10 µg/ml) or not were added to the 96-well plate

and cultured with anti-mouse CD28 (2 $\mu\text{g}/\text{ml}$) and rIL-2 (30 IU/ml) in RPMI 1640 medium. After cultured for 3 days, fresh culture medium with $1 \times$ Cell Stimulation Cocktail (plus protein transport inhibitors) was added to the plate for cytokine detection. And 6 h later, flow cytometry was applied to detect the activation of T cells.

T cells-mediated tumor killing assay

The detailed procedure for T cells-mediated tumor killing assay referred this article.²⁶ First, 4×10^4 4MOSC1 cells were seeded in 24-well plate and cultured for 24 h with PCSK9 inhibitor (10 $\mu\text{g}/\text{ml}$) or not. We then acquired CD8⁺ T cells from tumor infiltrated lymphocytes by flow cytometry sorting and added 4×10^5 CD8⁺ T cells to the 24-well plate. After cocultured for 12 h, Fura-2 acetoxymethyl ester (AM) and propidium iodide (PI) were added for live/dead-cell staining.

Antitumor effects of PF-06446846 in vivo

1×10^6 4MOSC1 cells (30 μl) were inoculated to the tongue of C57 BL/6J mouse to establish the syngeneic HNSCC 4MOSC1 tumor-bearing model. Six days later, when the tumor volume was notable, the mice were randomly divided into two groups: PBS and PF-06446846 (5mg/kg, i.p.). The PCSK9 inhibitor was injected every two days and that the tumor volume and body weight were recorded every two days.

To explore the synergic antitumor effect of PF-06446846 with $\alpha\text{PD-1}$ immunotherapy, syngeneic HNSCC 4MOSC1 tumor-bearing mouse model was established. Six days later, the mice were randomly divided into two groups: PBS, PF-06446846 (5mg/kg, i.p.), $\alpha\text{PD-1}$ (5mg/kg, i.p.) and PF-06446846+ $\alpha\text{PD-1}$ (equivalent dose of PF-06446846 and $\alpha\text{PD-1}$). Tumor volume was calculated by the following formula: $(V, \text{mm}^3) = 1/2 \times (\text{tumor length}) \times (\text{tumor width})$.² All mice were euthanized on day 16, and tumor and draining lymph node were dissected for further study.

Flow cytometry

The dissected tumor was processed by a gentle MACS Dissociator (Miltenyl Biotec, Germany) and lymph nodes were ground through a filter to obtain single cell suspension. Then, Lymphoprep (Stemcell, 07801) was applied to separate mononuclear cell from the obtained single cell suspension from tumor. Subsequently, the obtained single cell suspension was dispensed in 96-well U-bottom plate and stained with associated antibodies according to the manufacturer's protocols. Samples were analyzed by CytoFLEX S (Beckman Coulter, USA), and flow cytometry data was analyzed flowjo V10 software (flowjo LLC, USA). The gating strategy for immune cells was shown in [Figures S5](#) and [S6](#).

Total cholesterol detection assay

The Total Cholesterol Detection Kit was applied in this experiment. Excised tumor mixed with extracting solution (0.1g/1mL) was homogenized by ultrasonic at 4 $^{\circ}\text{C}$, and subsequently centrifugated at 10000 g for 10 min. Then, 20 μL extracted supernatant was used to detect the cholesterol level by the manufacturer's protocols. Finally, the standard curve was established and the total cholesterol level was calculated by the following formula: Total cholesterol = sample concentration \times volume of extracted supernatant/Tumor weight.

QUANTIFICATION AND STATISTICAL ANALYSIS

GraphPad Prism 9.0 was utilized to analyze the data. Unpaired T test was utilized to analyze the statistically significant differences between two groups. One-way analysis of variance (ANOVA) followed by Tukey's multiple comparisons and two-way ANOVA followed by Tukey's multiple comparisons was used to analyze statistically significant differences between more than two groups. We used Kaplan–Meier method to plot survival curve, and log-rank test was used to analyze the statistical significance of survival difference. The results are presented as the mean \pm standard error of the mean, and statistical significance was determined as $p < 0.05$ (* $P < 0.05$, ** $P < 0.01$, *** $P < 0.001$).